Chemical Science

ROYAL SOCIETY OF CHEMISTRY

EDGE ARTICLE

View Article Online
View Journal

Cite this: DOI: 10.1039/d5sc00316d

All publication charges for this article have been paid for by the Royal Society of Chemistry

3D printable organic room-temperature phosphorescent materials and printed real-time sensing and display devices†

Haodong Sun,‡[a] Yuxin Xiao,‡[a] Yunfei He,[a] Xiaoyu Wei,[a] Jindou Zou,[a] Yuanda Luo,[a] Yazhang Wu,[a] Jiaxin Zhao,[a] Vonika Ka-Man Au[d] and Tao Yu*[abc]

Polymer-based host–guest organic room-temperature phosphorescent (RTP) materials are promising candidates for new flexible electronic devices. Nowadays, the insufficient fabrication processes of polymeric RTP materials have hindered the development of these materials. Herein, we propose a strategy to realize 3D printable organic RTP materials and have successfully demonstrated real-time sensing and display devices through a Digital Light Processing (DLP) 3D printing process. We have designed and synthesized the molecules EtCzBP, PhCzBP and PhCzPM with A–D–A structures. The crucial role of strong intramolecular charge transfer (ICT) at the lowest triplet states in achieving bright photo-activated phosphorescence in polymer matrices has also been demonstrated. 3D printable RTP resins were manufactured by doping emissive guest molecules into methyl methacrylate (MMA). Based on these resins, a series of complex 3D structures and smart temperature responsive RTP performances were obtained by DLP 3D printing. Additionally, these RTP 3D structures have been applied in real-time temperature sensing and display panels for the first time. This work not only provides a guiding strategy for the design of emissive guest molecules to realize photo-activated RTP in poly(methyl methacrylate) (PMMA), but also paves the way for the development of 3D-printable real-time sensing structures and new-concept display devices.

Received 14th January 2025
Accepted 4th February 2025

DOI: 10.1039/d5sc00316d

rsc.li/chemical-science

Introduction

Room-temperature phosphorescent (RTP) materials that exhibit ultra-long lifetime emission have attracted enormous attention in recent years due to their great potential for applications in information storage,[1–3] anti-counterfeiting,[4–6] nonlinear optics,[7,8] bioimaging,[9–15] X-ray detection and imaging,[16,17] and light-emitting devices.[18–21] To avoid non-radiative transitions and achieve an ultra-long emissive process, a series of molecular design strategies have been proposed, such as forming H-aggregates,[22–24] strengthening intermolecular interactions,[25,26] manipulating the steric hindrances,[27] boosting the degree of crystallinity,[11,28] enhancing intermolecular electronic coupling,[29,30] and constructing polymer-based and small molecule-based host–guest systems.[1,4,31–42] Among these strategies, doping emissive guest molecules into polymer matrices to realize RTP has become a hotspot in recent years because of the intrinsic advantages of polymeric hosts, such as light weight, high flexibility, large-scale fabrication, and good mechanical stability. Besides, the rigid environment in the polymer-based matrix could effectively suppress the vibrational dissipation of excited states and promote the ultra-long emissive process.[43–45]

In recent years, a series of impressive examples of polymer-based host–guest RTP systems have been reported. Among these guest molecules, some exhibited intramolecular charge transfer (ICT) properties.[46–48] Other compounds lacking ICT characteristics could also demonstrate RTP after being doped in PMMA matrices.[1,49–53] However, the critical role of ICT states in promoting the RTP properties of poly(methylmethacrylate) (PMMA)-based doped RTP materials was not mentioned. Besides, the applications of polymer-based RTP materials have also been reported extensively. For instance, by incorporating various chromophores into the PMMA matrix and coating it with an oxygen-barrier layer, photoinduced programmable transparent organic luminescent tags for continuous

[a]Frontiers Science Center for Flexible Electronics (FSCFE), Shaanxi Institute of Flexible Electronics (SIFE), Shaanxi Institute of Biomedical Materials and Engineering (SIBME), Northwestern Polytechnical University (NPU), 127 West Youyi Road, Xi'an, 710072, China. E-mail: iamtyu@nwpu.edu.cn

[b]Key Laboratory of Flexible Electronics of Zhejiang Province, Ningbo Institute of Northwestern Polytechnical University, 218 Qingyi Road, Ningbo, 315103, China

[c]Shenzhen Research Institute of Northwestern Polytechnical University, 45 Gaoxin Nanjiu Road, Shenzhen, 518063, China

[d]Department of Science and Environmental Studies, The Education University of Hong Kong, 10 Lo Ping Road, New Territories, Tai Po, Hong Kong, China

† Electronic supplementary information (ESI) available: Synthetic procedures, experimental details and supplemental figures. CCDC 2189250, 2299673 and 2341195. For ESI and crystallographic data in CIF or other electronic format see DOI: https://doi.org/10.1039/d5sc00316d

‡ These authors made equal contributions to this article.

information storage and erasure were designed.[1,52,54–56] Taking advantage of the oxygen-sensitive characteristics of polymer-based RTP materials, Li and coworkers reported their applications in oxygen leak testing and microcrack detection.[51] Nevertheless, the applications of polymer-based RTP materials were mainly demonstrated in thin films, and thus, the construction of precisely prescribed complex 3D geometries with smart RTP properties became an appealing issue.[1,2,5,51–53,57–59] Digital Light Processing (DLP) 3D printing offers the ability to fabricate complex RTP structures by utilizing digital mask projection to trigger localized photopolymerization.[60,61] Through the DLP-based 3D printing method, it becomes feasible to realize structure–function integrated RTP 3D structures that show responsiveness to multiple stimuli.

Herein, we have designed and synthesized a series of new guest molecules to fabricate polymer-based RTP materials, named EtCzBP, PhCzBP, and PhCzPM. Upon doping into PMMA, EtCzBP and PhCzBP exhibited obvious photo-activated RTP performance, while no RTP was observed for PhCzPM. Photophysical studies and time-dependent density functional theory (TD-DFT) calculations were performed to reveal the origins of the RTP emissions and the photo-activated properties. DLP printable photo-activated RTP resins were achieved by doping EtCzBP into MMA based resins and a series of complex 3D structures with RTP properties were also successfully achieved. For the printed 3D structures, the RTP duration and ON/OFF states were sensitive and readily tunable depending on the surrounding temperature. Accordingly, 3D-printable real-time temperature sensing and new-concept displays were fabricated based on these new 3D printable resins.

Results and discussion

The compounds EtCzBP, PhCzBP and PhCzPM (Fig. 1a) were synthesized according to the methods listed in the ESI (Fig. S2–S7†), and were characterized by ^{1}H nuclear magnetic resonance (NMR) spectroscopy and high-resolution mass spectroscopy. The ultraviolet (UV)–visible (vis) absorption spectra, normalized steady-state emission spectra and delayed emission spectra of EtCzBP, PhCzBP and PhCzPM in dilute solutions (1.0×10^{-5} M) are shown in Fig. 1b and d. For EtCzBP, the higher energy absorption bands at *ca.* 313 nm were assigned to π–π* transitions, whereas the lower absorption bands at *ca.* 354 nm originated from intramolecular charge transfer (ICT) transitions according to previous reports with similar structures.[62] Similarly, PhCzBP exhibited π–π* transitions at *ca.* 316 nm and ICT transitions at *ca.* 361 nm. For PhCzBP and EtCzBP, the ICT transition characteristics could be further demonstrated by the Lippert–Mataga equation according to the bathochromic shift from 412 nm to 517 nm with increasing solvent polarity (Fig. S8 and S9 and Tables S1 and S2†).[63] For PhCzPM, two absorption bands were observed at *ca.* 299 nm and *ca.* 335 nm. The emission bands originating from locally excited (LE) and ICT transitions could be observed in ethyl acetate solvent (Fig. S10†). Compared to EtCzBP and PhCzBP, PhCzPM exhibited a blue-shifted absorption peak, resulting from its weaker electron-donating capability.[64,65] The calculated results based on TD-DFT further demonstrated the weaker electron-donating capability of PhCzPM, leading to a lower highest occupied molecular orbital (HOMO) energy level (Fig. S17†).[66–68] Besides, the hybridization of the HOMO and lowest unoccupied molecular orbital (LUMO) of PhCzPM enhanced the component of the π–π* transition.[69] The crystalline samples EtCzBP, PhCzBP and PhCzPM showed a structureless emission band located at *ca.* 479 nm, 484 nm and 478 nm (photoluminescence quantum yield (PLQY) = 14.7%, 5.3% and 2.0%), respectively (Fig. S11†). Single crystal analysis showed that there were various kinds of hydrogen bonds (2.468 Å–2.657 Å) and C–H···π interactions (2.761 Å–2.900 Å) for one EtCzBP molecule with two conformations. In contrast, only two types of hydrogen bonds (2.497 Å and 2.469 Å) were observed in PhCzBP and one type of hydrogen bond (2.416 Å) exists in PhCzPM (Fig. S14–S16†). The intermolecular interactions could efficiently restrict the vibrations and rotations of excited states and promote the PLQYs in the solid states.[70,71] Therefore, the higher PLQY for EtCzBP might be attributed to the relatively stronger intermolecular interactions in the molecular packing arrangement. The corresponding time-resolved decay curves proved that all the compounds were typical fluorescent materials (Fig. S11†). Besides, the non-centrosymmetric structures and abundant intermolecular hydrogen bonds resulted in the bright mechanoluminescence of crystalline EtCzBP upon external force stimulation (Fig. S12–S14†).[63] In 2-methyltetrahydrofuran (2-MeTHF) glass at 77 K, the delayed spectra of EtCzBP, PhCzBP and PhCzPM showed structured emission bands with maxima at 532, 528 and 452 nm, respectively. The emission bands were assignable to phosphorescence.

Furthermore, PMMA (Mw ∼ 200 000) was selected as a polymer matrix that could provide a rigid environment to protect triplet excitons. The films were prepared using the method illustrated in the ESI† and the thickness was about 450 μm. As shown in Fig. 1e, f and h, photo-activated RTP emission was achieved by doping EtCzBP and PhCzBP into the PMMA matrix with a concentration of 5 wt% (named EtCzBP@PMMA and PhCzBP@PMMA). For EtCzBP@PMMA, a Gaussian band at *ca.* 477 nm was detected under UV excitation (365 nm). Under persistent UV excitation (365 nm, 3.46 mW cm^{-2}) for 4 s, low-energy emission bands at *ca.* 498 nm and 537 nm appeared. Strong green afterglow lasting more than 2 s could be observed by the naked eye after turning off the excitation, and the lifetime reached 189 ms (Fig. S19†). The fluorescence and phosphorescence quantum yields after UV irradiation were 4.6% and 3.2%, respectively.[72] After doping EtCzBP into the PMMA matrix with different average molecular weights of 100 000 g mol^{-1} and 150 000 g mol^{-1}, the doped polymer films still exhibited similar RTP performance (Fig. S22†). PhCzBP@PMMA films also exhibited a similar photo-activated RTP process (Fig. 1f and S23†). Based on the photophysical analysis, it was revealed that EtCzBP and PhCzBP showed essentially the same emission bands in the PMMA matrix and in the 2-MeTHF glass state (77 K, 1.0×10^{-5} M) as shown in Fig. 1. It was preliminary demonstrated that the compounds were well dispersed in the PMMA polymer matrix. To provide further substantiation, optical microscopy and laser scanning confocal microscopy (LSCM) were performed on the

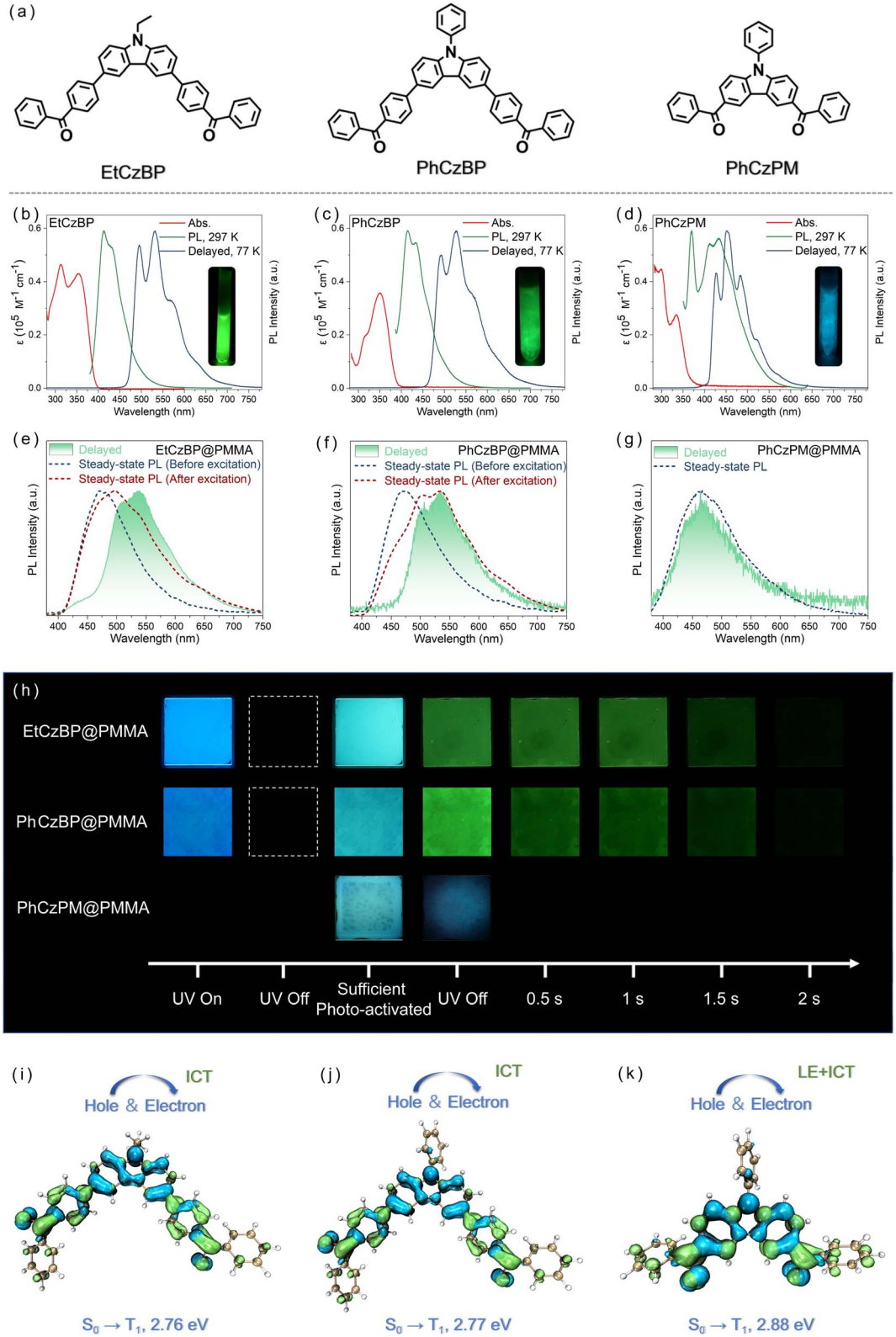

Fig. 1 Compound structure, hole and electron distributions and photophysical properties of the phosphorescence emitters in dilute solvents and in the polymer matrix. (a) Chemical structures of EtCzBP, PhCzBP and PhCzPM. UV-Vis absorption, normalized steady-state PL and delayed (delayed time = 8 ms) spectra for (b) EtCzBP, (c) PhCzBP and (d) PhCzPM; inset: the phosphorescent photograph at 77 K after UV excitation. Steady-state PL spectra before UV excitation and after UV excitation, and delayed (delayed time = 8 ms) spectra for (e) EtCzBP@PMMA, (f) PhCzBP@PMMA and (g) PhCzPM@PMMA. (h) Photographs of the EtCzBP@PMMA, PhCzBP@PMMA and PhCzPM@PMMA films under UV excitation (first column)and after turning off the UV excitation (second column) before being photo-activated (λ_{ex} = 365 nm), upon a sufficient photo-activated process (third column) and photo-activated RTP (fourth column and onwards). Electron–hole isosurface of the $S_0 \rightarrow T_1$ transition for (i) EtCzBP, (j) PhCzBP and (k) PhCzPM (isovalue = 0.001). The blue and green isosurfaces correspond to the hole and electron distributions, respectively.

doped polymer films (Fig. S24†). The results showed that the PMMA films doped with guest molecules were very uniform and without aggregated areas.[73,74] These results further proved the good dispersion of these compounds in the doped PMMA films. Therefore, the photo-activated phosphorescence at *ca.* 508 nm and 536 nm was attributed to the phosphorescent components. However, no obvious photo-activated RTP process was observed by dispersing PhCzPM in PMMA with a concentration of 5 wt%, even after prolonged excitation. For PhCzPM@PMMA films, an emission band at *ca.* 462 nm was observed under UV excitation, as shown in Fig. 1g. Upon termination of UV excitation, faint and brief phosphorescence with a lifetime of 103 μs was observed (Fig. S26†). As shown in Fig. 1h, EtCzBP@PMMA, PhCzBP@PMMA and PhCzPM@PMMA films showed photo-activated RTP under UV excitation (λ_{ex} = 365 nm). The delayed spectrum exhibited a similar profile to that observed in 2-MeTHF glass at 77 K. Specifically, the shortened distance between the carbazole and carbonyl groups in PhCzPM, compared to EtCzBP and PhCzBP, may influence its ability to initiate a photo-activated RTP process. The observed weak photo-activated phosphorescence performance of PhCzPM@PMMA films may be attributed to the distinct modes of electron transition in the excited state.

To further investigate the mechanism of photo-activated RTP of phosphorescent emitters in the polymer matrix, theoretical calculations based on density functional theory (DFT) were carried out at the B3LYP/6-311G* level (Fig. 1i–k and S17, and Tables S3–S5†).[75,76] The hole and electron distributions of the $S_0 \rightarrow T_1$ transition for EtCzBP and PhCzBP indicated that the holes and electrons were located in separated regions. It indicated the presence of ICT character from the electron-rich donor carbazole to the electron-deficient benzophenone moieties. The intense ICT transition was also supported by the large bathochromic shift of EtCzBP and PhCzBP with increasing solvent polarity (Fig. S8 and S9†). For PhCzPM, the shorter distance between the carbazole group and the benzophenone group led to the hybridization of the electrons and holes around the carbonyl groups in the $S_0 \rightarrow T_1$ transition. It suggested that the lowest triplet excited states displayed mainly locally excited (LE) state and ICT state characters. Upon excitation, PhCzPM exhibited emission peaks related to LE and CT transitions in toluene and ethyl acetate solvents (Fig. S10†). Besides, it was noteworthy that the spin–orbit coupling constants (ξ) of S_1 to T_n for monomers EtCzBP and PhCzBP were found to be basically similar to those of the monomer PhCzPM, indicating a similar efficient intersystem crossing (ISC) process for the generation of triplet excitons (Fig. S18†). However, even after longer excitation, photo-activated RTP emission could hardly be observed in PhCzPM@PMMA films. Therefore, we believed that the different transition modes present in the lowest triplet excited states have played significant roles in the photo-activated phosphorescent process.

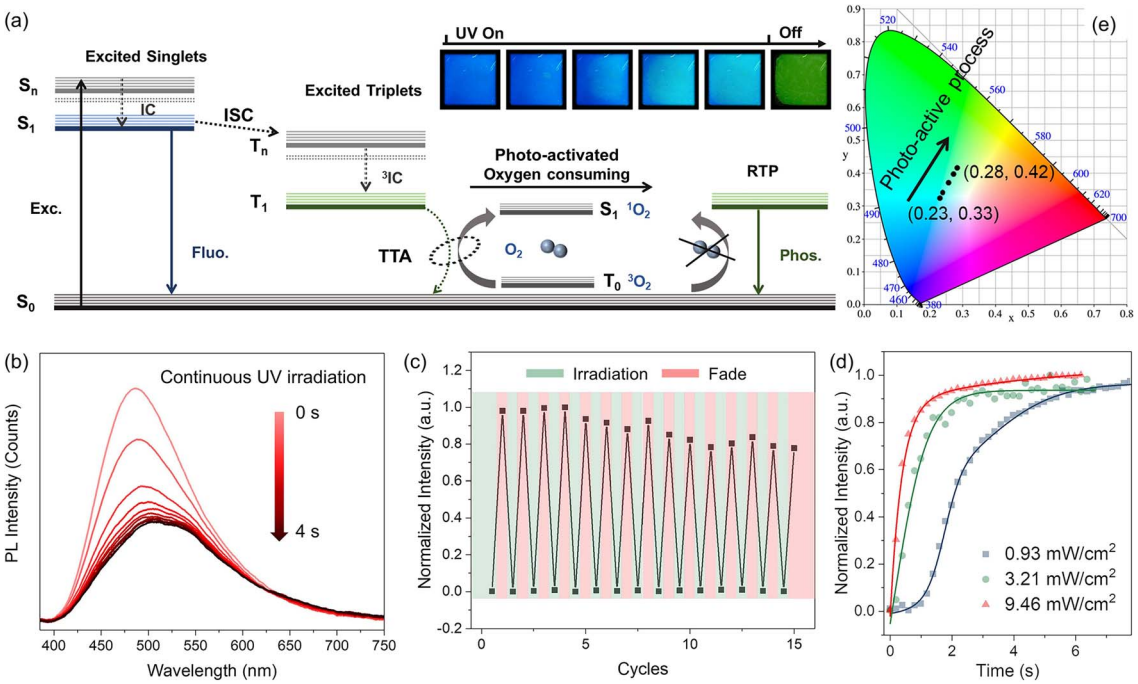

Fig. 2 Mechanism and photo-activated RTP process of EtCzBP@PMMA films. (a) Jablonski diagram for the possible internal mechanism of molecular oxygen consumption under UV irradiation in the photo-activated RTP effect. Exc. stands for excitation, IC for internal conversion, ISC for intersystem crossing, TTA for triplet–triplet annihilation, Fluo. for fluorescence, and Phos. for phosphorescence. (Inset) Photographs of EtCzBP@PMMA films under continuous UV irradiation and after ceasing irradiation. (b) Steady-state PL spectra of EtCzBP@PMMA films under sustained UV light irradiation (λ_{ex} = 365 nm) (3.21 mW cm^{-2}). (c) Normalized phosphorescence intensity at 536 nm of EtCzBP@PMMA films upon alternating UV light irradiation (3.21 mW cm^{-2}) for 10 s and ceasing UV irradiation for 5 min. (d) Time-dependent normalized phosphorescence intensity at 536 nm of EtCzBP@PMMA films under UV irradiation with various power densities. (e) The corresponding CIE chromaticity diagram for the PL emission of EtCzBP@PMMA under sustained UV light irradiation.

As shown in Fig. 2b, for EtCzBP@PMMA films, the emission bands at *ca.* 508 nm and 536 nm were negligible at the initial stage but became prominent upon continuous UV excitation for 4 s (3.46 mW cm^{-2}). The decreased PL intensity with increasing UV irradiation duration was because the UV irradiation process intensified the molecular motion, leading to an increased nonradiative transition process (Fig. S20 and S21†).[77] The corresponding CIE chromaticity coordinates shifted from (0.23, 0.32) to (0.28, 0.42) (Fig. 2e). The photographs in Fig. 2a also manifested the photo-activated RTP process. Subsequently, the stability of the photo-activated RTP photoswitching performance was thoroughly assessed (Fig. 2c). After undergoing 15 repeated cycles of UV irradiation turning on and off, ~80% of the initial photo-activated phosphorescent intensity was maintained. The photo-activated RTP performance could still be efficiently achieved. Fig. S25a† shows that the doped PMMA films can still exhibit stable RTP even after multiple photo-activation processes, which could be further used for multiple information writing and erasure. Besides, the RTP lifetime of the doped polymer films remained stable under different UV irradiation durations (Fig. S25b†). The stable photo-activated RTP performance laid the foundation for extensive and advanced applications in various fields. Moreover, the photo-activated RTP behavior was highly related to the intensity of excitation UV light. Impressively, the activation time of EtCzBP@PMMA films gradually decreased as the UV light power density increased from 0.93 to 9.46 mW cm^{-2} (Fig. 2d). The gradually increased phosphorescent component during the photo-activated process was in connection with the oxygen existing in the polymer matrix (Fig. 2a).[1] The transmittance results of the solution or films containing both PMMA and EtCzBP provided evidence in support of this hypothesis (Fig. S28†). The tetrahydrofuran (THF) solution containing both PMMA and EtCzBP exhibited notable changes in the transmittance and colour after UV excitation for 20 minutes, displaying increased absorption in the blue wavelength region. Similarly, for EtCzBP@PMMA films, the transmission decreased and the colour of the films changed to yellow after UV excitation. This observation was consistent with the well-known phenomenon of yellowing as an indication of polymer oxidation. After fabrication, the EtCzBP@PMMA films contained some triplet ground state oxygen. In the initial stage of UV irradiation, the populated triplet excitons of EtCzBP would be quenched by triplet oxygen inside the films and singlet oxygen

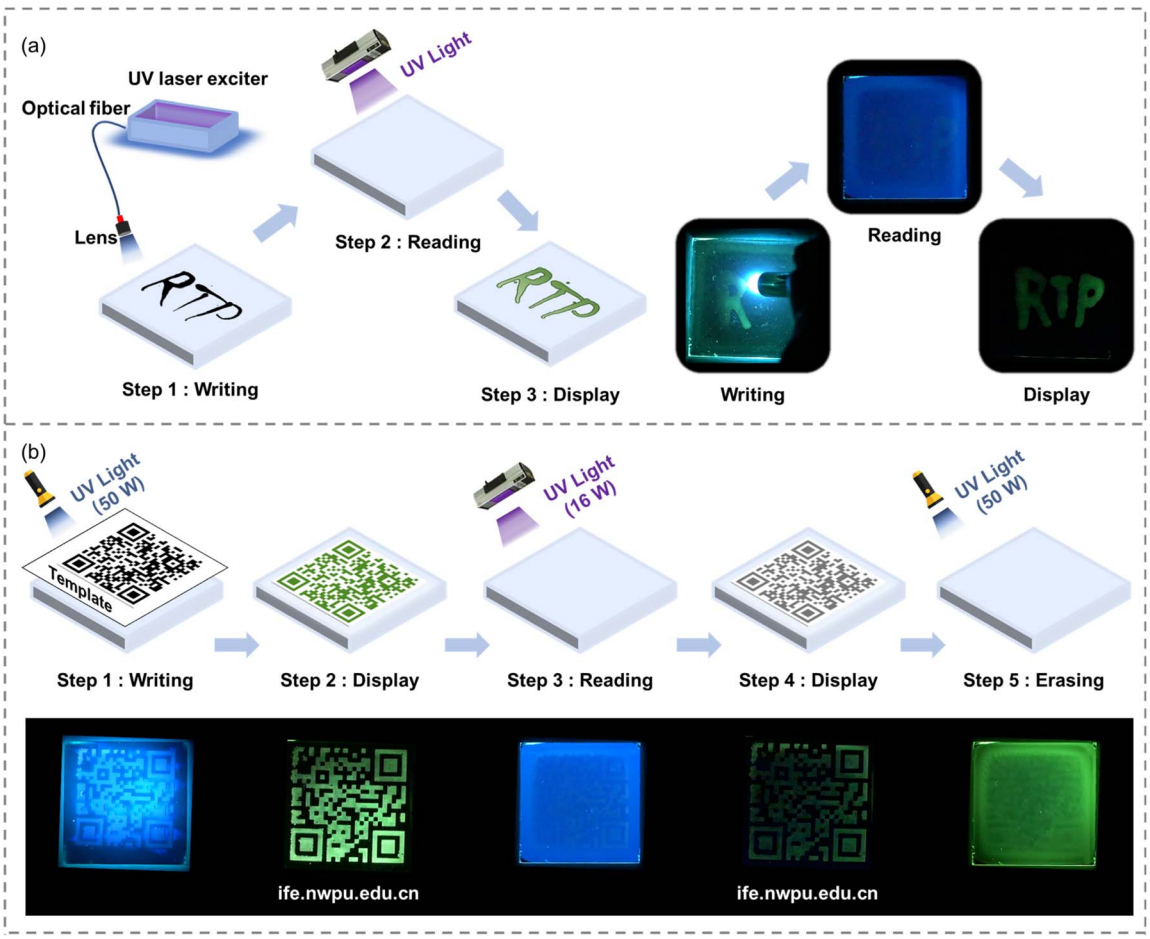

Fig. 3 Applications of photo-activated phosphorescent films. (a) Schematic illustration (left) and photographs (right) of their application for light information input (9.46 mW cm^{-2}, 298 K). (b) Schematic diagrams (up) and photographs (down) of the storage, reading and erasing process of QR codes.

was produced *via* a triplet–triplet annihilation (TTA) process. After constant UV irradiation, the triplet oxygen was totally consumed by the excited triplet excitons of EtCzBP, which could decay through a radiative process, leading to the appearance of phosphorescence. In the photoactivated process, the singlet oxygen could interact with PMMA, resulting in the oxidation and yellowing of PMMA (Fig. S28†).[1] The TTA process between the triplet excitons of EtCzBP and triplet oxygen that accelerates the generation of excited singlet oxygen was also proved by the ultraviolet absorption spectrum of EtCzBP and DPBF (1,3-diphenylisobenzofuran) (Fig. S29†).

Taking advantage of the remarkable photo-activated RTP properties of the EtCzBP@PMMA films, afterglow patterns were easily recorded by persistent UV illumination. For instance,

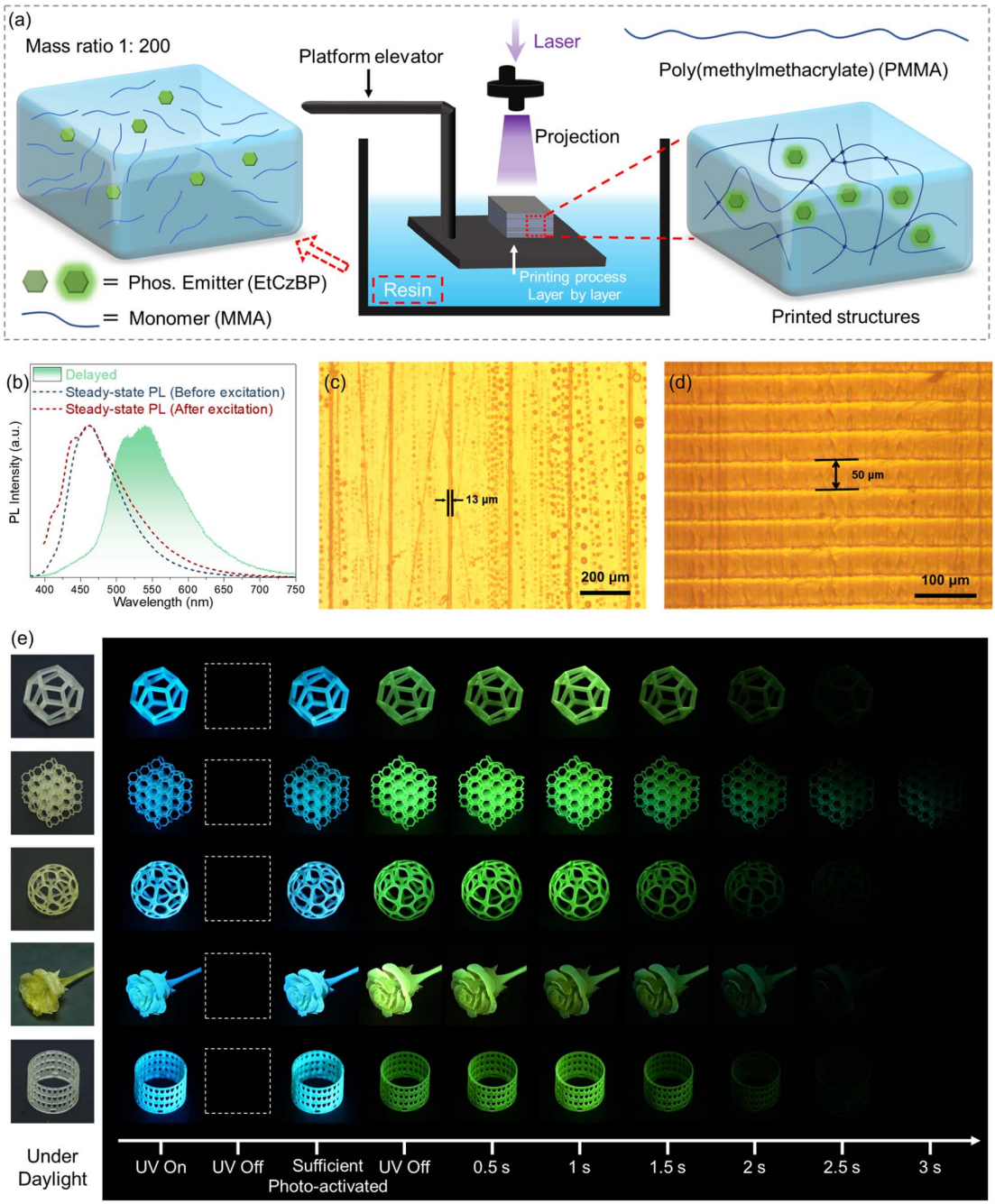

Fig. 4 Construction of complex 3D structures with photo-activated RTP properties by digital light processing 3D printing. (a) Illustration of the photo-activated RTP materials using DLP 3D printing technology. (b) Delayed (delayed time = 8 ms) spectrum, steady-state PL spectra before UV (dashed line in blue) and after UV excitation (dashed line in red) of the 3D structures. (c) Microscopic images of the striped patterns with a 13 μm width printed with the printable resins. (d) Microscopic images of the printed 3D structures in the *Z*-direction. (e) Photographs of various printed complex 3D structures under daylight, UV excitation (before and after sufficient photo-activation) and after termination of UV excitation (9.46 mW cm^{-2}, 298 K, and UV irradiation for 3 min).

"RTP" characters could be written on the EtCzBP@PMMA films by using a light optical fiber. Under flash UV excitation, the characters could be observed (Fig. 3a and Movies S1†). In addition, information such as a Quick Response (QR) code could be clearly printed on the films with a mask (Fig. 3b and Movies S2†). The QR code could then be read under flash UV light excitation (16 W) (Fig. 3b). Moreover, the QR code information could be erased by activating the phosphorescence of the entire film with persistent UV irradiation (50 W). To date, most applications for organic RTP materials have focused on two-dimensional flexible films, but complex structures with smart RTP properties have seldom been reported.[45,78] Herein, the molecule EtCzBP was selected as the dopant due to its high PLQY and great RTP potential among the three molecules and by doping EtCzBP phosphorescent molecules into a MMA based resin with an optimized concentration of 0.5 wt% (Fig. S30†), a DLP printable resin was achieved. EtCzBP molecules have been proved to act as light absorbers in EtCzBP@PMMA inks to improve printing precision (Fig. S31†). Based on the rapid light curing of liquid resins, DLP 3D printing has the advantage of producing complex 3D objects with high resolution geometry and printing efficiency.[79–82] As depicted in Fig. 4a, the prepared liquid resins were directly used in DLP 3D printing. The solidified 3D structures consisted of cross-linked PMMA macromolecular chains and dispersed EtCzBP emitters, forming a cohesive network within the matrix. Based on the resin, different types of complex structures, such as an exquisite flower, a meshy sphere, a regular dodecahedron, a hollow cube, *etc.*, with photo-activated RTP properties were printed through DLP 3D printing (Fig. 4e). As shown in Fig. 4b, under persistent UV excitation, the steady-state emission spectrum of the 3D structures displayed a broad emission band, and a bright afterglow could be observed after ceasing UV light. The afterglow could last more than 2 s with a lifetime of 188 ms (Fig. S27†). The delayed emission spectrum was in good accordance with that of EtCzBP in 2-MeTHF at 77 K. Besides, the obtained EtCzBP@PMMA resins enabled the fabrication of high-resolution 3D structures with RTP performance (up to 13 μm in the *X*-direction in Fig. 4c). The uniform layer thickness of the resulting 3D structures matched the preset slice thickness of *ca.* 50 μm (Fig. 4d). The phosphorescence-emitting region of the 3D structures is in the range of 50–100 μm from the surface under UV excitation (Fig. S36†). This suggested that utilizing DLP 3D printing to fabricate complex 3D structures with RTP emission was a very feasible and dependable approach. Based on the high precision manufacturing process, a series of complex 3D structures with temperature-responsive RTP properties were prepared. Meanwhile, the successful fabrication of these structures provides the necessary prerequisites for applications such as real-time temperature sensing 3D structures and new-concept RTP-based displays.

Although the application of organic phosphorescent materials has made great progress in recent years, phosphorescent sensing and display based on complex structures have rarely been reported. By doping EtCzBP emitters into MMA based resins, an ink capable of DLP 3D printing was obtained. Compared with fluorescence, organic RTP was much more sensitive to the surrounding temperature, due to the long-lasting decay processes and intense dissipation of triplet excitons.[25,26] The obtained DLP-printed 3D structures with RTP performance also exhibited obvious temperature-responsive characteristics. By gradually enhancing the surrounding temperature from 20 °C to 80 °C, the phosphorescent lifetime of the printed 3D structures gradually decreased from 229 ms to 87 ms (Fig. S32–S35†). Based on that, the temperature of the 3D printing structure could be evaluated by the RTP lifetime. Therefore, phosphorescence-based temperature real-time sensing and display structures based on prescript structures were successfully fabricated (Movie S3†). As shown in Fig. 5a, the spiral hollow structure was obtained by DLP 3D printing, and the hollow structure could be used as a channel for fluid flow. The real-time temperature of the fluid flow could be directly sensed by measuring the duration of the afterglow. For instance, when liquid at ambient temperature (*ca.* 21 °C) flowed through the spiral hollow pipes, simultaneous disappearance of afterglow was observed in all three spirals after turning off the UV light. When hot liquid (*ca.* 65.7 °C) flowed through the spiral hollow pipes, it would gradually be cooled from *ca.* 65.7 °C to *ca.* 31.9 °C according to the infrared images in Fig. 5a. The cooling process of the liquid was visibly manifested according to the different phosphorescent durations at different positions of the 3D printed spiral pipes. The duration of the afterglow could not be detected by the naked eye at a temperature of 65.7 °C, while it gradually increased to 0.3 s and 0.8 s at temperatures of 49.7 °C and 31.9 °C, respectively. As shown in Fig. S37,† when the spiral hollow pipes were covered with a transparent glass (1.1 mm), the infrared camera failed to display the real-time temperature of the structure properly through the glass plate. However, the temperature signal of the structure could still be captured through the glass *via* phosphorescence. Therefore, real-time temperature sensing *via* monitoring the duration of the afterglow in the designed 3D-printed structures could effectively address the limitation of the infrared camera's inability to transmit signals through certain media like glass. Based on these results, real-time temperature sensing *via* monitoring the duration of the afterglow for the designed 3D-printed structures has been demonstrated. According to the temperature-dependent RTP ON/OFF switches, an RTP display array was designed and fabricated by the DLP 3D printing method, as shown in Fig. 5b. In the RTP array, each pixel was represented by a mini-channel fabricated *via* DLP 3D printing (Fig. 5b). The temperature of each pixel could be easily and readily manipulated by flowing water or gas flow through the mini-channels (Movie S4†). Thus, as shown in Fig. 5b, through controlling the temperature of different mini-channels, various letters "N", "W", "P", "U", "I", "F", and "E" and a heart symbol were alternatively displayed on the 6 × 6 pixel array after turning off the UV excitation. In addition, the displays could be easily extended to larger ones by increasing the number of pixel units. For instance, a more complex emoji pattern could be shown on a larger display with 12 × 12 pixels. These results, derived from the utilization of RTP 3D-printable resins, have presented a new approach for constructing complex 3D structures that are capable of real-time temperature sensing and useful for new-

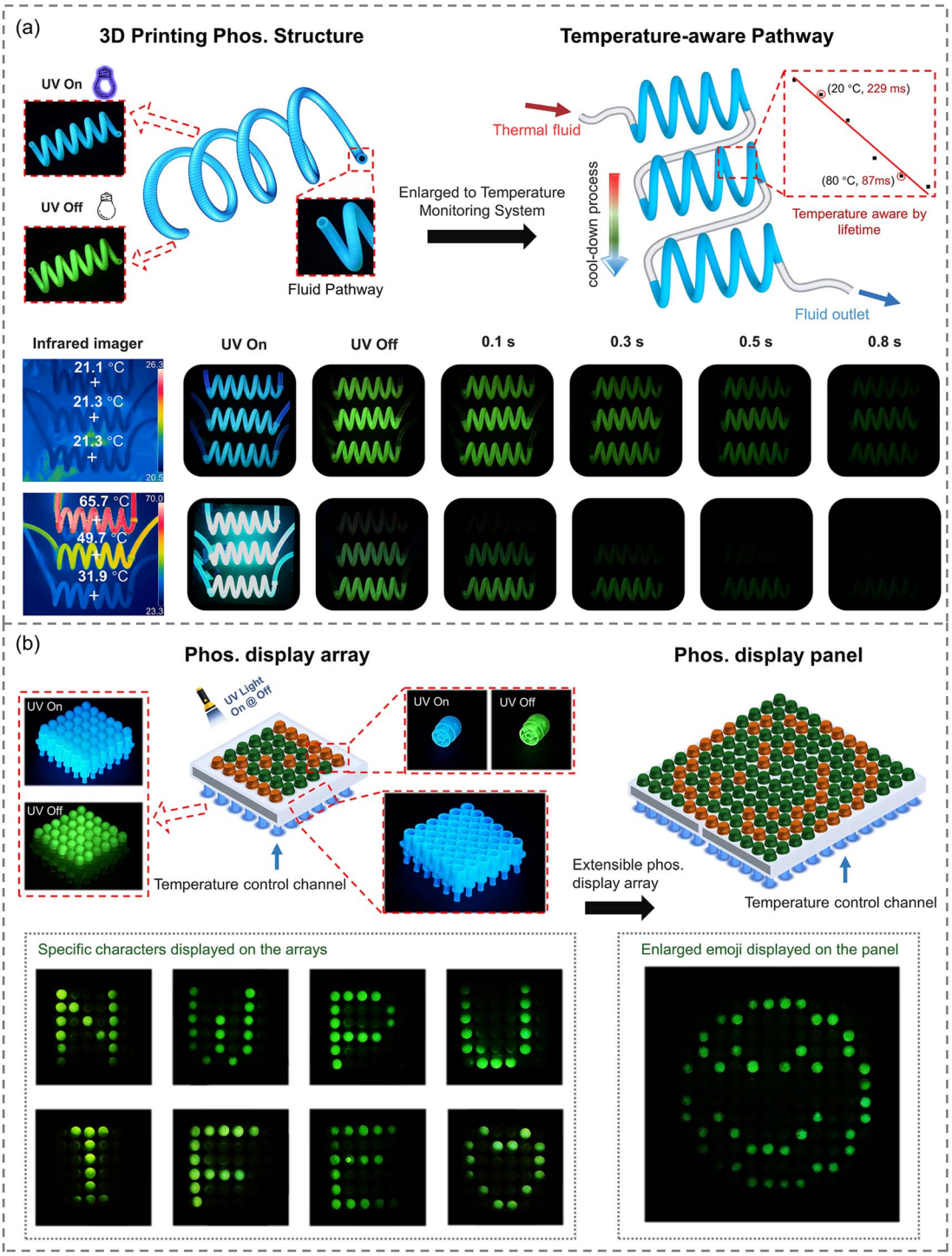

Fig. 5 Phosphorescent temperature sensing and large area panel display based on 3D printed complex structures. (a) (Top) Schematic diagram of printed spiral hollow structure and corresponding temperature self-monitoring; inset: fluorescent and afterglow photographs of the printed spiral hollow structure. (Bottom) Infrared images, fluorescent and afterglow photographs of spiral hollow structures after the injection of ambient fluids and high temperature fluids, and the corresponding temperature points of the spiral structures. (b) (Top) Schematic diagrams of phosphorescent display arrays and the enlarged display panel (298 K), inset: the fluorescent and afterglow images for printed 3D phosphorescent pixels, temperature control modules, and the constructed phosphorescent display arrays. The constructed phosphorescent display arrays could enlarge to display panels. (Bottom) Various letters or patterns ("N", "W", "P", "U", "I", "F", "E", and "♡") and emoji appeared on the phosphorescent display array and panel after ceasing UV light, respectively (9.46 mW cm^{-2}, 298 K, and UV irradiation for 3 min).

concept display devices. Long-term storage of 3D printed structures in high humidity environments can affect or even extinguish their ambient RTP, which needs to be improved in the future with the development of more materials that are not sensitive to ambient humidity.

Conclusions

In conclusion, we have devised a strategy to prepare 3D-printable organic RTP materials and successfully realized real-time sensing and display devices through DLP 3D printing processes. Three phosphorescent guest emitters, PhCzBP, EtCzBP and PhCzPM, were designed and synthesized. By doping these emitters into the PMMA polymer matrix, the EtCzBP@PMMA and PhCzBP@PMMA films exhibited decent RTP performance with lifetimes of 189 ms and 256 ms, respectively. It was proved that the compounds EtCzBP and PhCzBP exhibited well-separated electrons and holes in triplet excited states, which could in turn promote the RTP performance in the polymeric host. The polymer matrix of PMMA not only exhibited a suitable energy level in processing and application, but also provided a rigid micro-environment to suppress the non-radiative decay to induce RTP. Besides, the mechanism of the photo-activated RTP process was well explained. Accordingly, the input and output of light information could be achieved easily based on the photo-activated characteristics and photo-response diversity of the material. Through DLP 3D printing techniques, a series of complex 3D structures with decent photo-activated RTP properties were precisely fabricated, and structure–function integrated RTP 3D structures were obtained. Based on the temperature sensing and ON/OFF switch properties of the RTP emission, real-time temperature sensing and new-concept displays based on complex 3D structures were demonstrated. This work presents a new and efficient strategy to construct 3D structures with remarkable RTP properties and paves the way for organic RTP in potential applications in real-time temperature sensing and display technologies.

Data availability

The authors confirm that the data supporting the findings of this study are available within the article and its ESI.† Raw data that support the findings of this study are available from the corresponding author, upon reasonable request.

Author contributions

T. Yu. conceived the project and experiments. H. Sun designed the molecules, H. Sun and Y. Xiao conducted the experiment and wrote the manuscript. V. K. Au helped revise the manuscript. Y. He and J. Zou performed the 3D printing process. X. Wei, Y. Luo, Y. Wu, and J. Zhao discussed the results. All authors contributed to writing the manuscript.

Conflicts of interest

There are no conflicts to declare.

Acknowledgements

Haodong Sun and Yuxin Xiao contributed equally. The authors gratefully acknowledge financial support from the NSF of China (62275217), the Fundamental Research Funds for the Central Universities, the Natural Science Basic Research Program of Shaanxi Province (2024JC-JCQN-51) and the Innovation Foundation for Doctor Dissertation of Northwestern Polytechnical University (No. CX2022081 and CX2023106). V. K.-M. A. acknowledges support from the Early Career Scheme (ECS) from the Research Grants Council of the Hong Kong Special Administrative Region, P. R. China (EdUHK 28300220).

Notes and references

1 M. Gmelch, H. Thomas, F. Fries and S. Reineke, *Sci. Adv.*, 2019, **5**, eaau7310.
2 D. Li, J. Yang, M. Fang, B. Z. Tang and Z. Li, *Sci. Adv.*, 2022, **8**, eabl8392.
3 H. Peng, G. Xie, Y. Cao, L. Zhang, X. Yan, X. Zhang, S. Miao, Y. Tao, H. Li, C. Zheng, W. Huang and R. Chen, *Sci. Adv.*, 2022, **8**, eabk2925.
4 Y. Su, S. Z. F. Phua, Y. Li, X. Zhou, D. Jana, G. Liu, W. Q. Lim, W. K. Ong, C. Yang and Y. Zhao, *Sci. Adv.*, 2018, **4**, eaas9732.
5 X. Yao, H. Ma, X. Wang, H. Wang, Q. Wang, X. Zou, Z. Song, W. Jia, Y. Li, Y. Mao, M. Singh, W. Ye, J. Liang, Y. Zhang, Z. Liu, Y. He, J. Li, Z. Zhou, Z. Zhao, Y. Zhang, G. Niu, C. Yin, S. Zhang, H. Shi, W. Huang and Z. An, *Nat. Commun.*, 2022, **13**, 4890.
6 Z. Xie, X. Zhang, H. Wang, C. Huang, H. Sun, M. Dong, L. Ji, Z. An, T. Yu and W. Huang, *Nat. Commun.*, 2021, **12**, 3522.
7 S. Hirata, K. Totani, T. Yamashita, C. Adachi and M. Vacha, *Nat. Mater.*, 2014, **13**, 938–946.
8 S. Hirata and M. Vacha, *J. Phys. Chem. Lett.*, 2017, **8**, 3683–3689.
9 S. M. A. Fateminia, Z. Mao, S. Xu, Z. Yang, Z. Chi and B. Liu, *Angew. Chem., Int. Ed.*, 2017, **56**, 12160–12164.
10 A. Nicol, R. T. K. Kwok, C. Chen, W. Zhao, M. Chen, J. Qu and B. Z. Tang, *J. Am. Chem. Soc.*, 2017, **139**, 14792–14799.
11 F. Xiao, H. Gao, Y. Lei, W. Dai, M. Liu, X. Zheng, Z. Cai, X. Huang, H. Wu and D. Ding, *Nat. Commun.*, 2022, **13**, 186.
12 G. Zhang, G. M. Palmer, M. W. Dewhirst and C. L. Fraser, *Nat. Mater.*, 2009, **8**, 747–751.
13 Q. Dang, Y. Jiang, J. Wang, J. Wang, Q. Zhang, M. Zhang, S. Luo, Y. Xie, K. Pu, Q. Li and Z. Li, *Adv. Mater.*, 2020, **32**, 2006752.
14 X. Zhen, Y. Tao, Z. An, P. Chen, C. Xu, R. Chen, W. Huang and K. Pu, *Adv. Mater.*, 2017, **29**, 1606665.
15 Y. Wang, H. Gao, J. Yang, M. Fang, D. Ding, B. Z. Tang and Z. Li, *Adv. Mater.*, 2021, **33**, 2007811.
16 X. Wang, W. Sun, H. Shi, H. Ma, G. Niu, Y. Li, J. Zhi, X. Yao, Z. Song, L. Chen, S. Li, G. Yang, Z. Zhou, Y. He, S. Qu, M. Wu, Z. Zhao, C. Yin, C. Lin, J. Gao, Q. Li, X. Zhen, L. Li, X. Chen, X. Liu, Z. An, H. Chen and W. Huang, *Nat. Commun.*, 2022, **13**, 5091.
17 X. Wang, H. Shi, H. Ma, W. Ye, L. Song, J. Zan, X. Yao, X. Ou, G. Yang, Z. Zhao, M. Singh, C. Lin, H. Wang, W. Jia, Q. Wang,

J. Zhi, C. Dong, X. Jiang, Y. Tang, X. Xie, Y. Yang, J. Wang, Q. Chen, Y. Wang, H. Yang, G. Zhang, Z. An, X. Liu and W. Huang, *Nat. Photonics*, 2021, **15**, 187–192.
18 R. Kabe, N. Notsuka, K. Yoshida and C. Adachi, *Adv. Mater.*, 2016, **28**, 655–660.
19 J. Lee, H.-F. Chen, T. Batagoda, C. Coburn, P. I. Djurovich, M. E. Thompson and S. R. Forrest, *Nat. Mater.*, 2016, **15**, 92–98.
20 C.-F. Chang, Y.-M. Cheng, Y. Chi, Y.-C. Chiu, C.-C. Lin, G.-H. Lee, P.-T. Chou, C.-C. Chen, C.-H. Chang and C.-C. Wu, *Angew. Chem., Int. Ed.*, 2008, **47**, 4542–4545.
21 J. Wang, X. Gu, H. Ma, Q. Peng, X. Huang, X. Zheng, S. H. P. Sung, G. Shan, J. W. Y. Lam, Z. Shuai and B. Z. Tang, *Nat. Commun.*, 2018, **9**, 2963.
22 E. Lucenti, A. Forni, C. Botta, L. Carlucci, C. Giannini, D. Marinotto, A. Pavanello, A. Previtali, S. Righetto and E. Cariati, *Angew. Chem., Int. Ed.*, 2017, **56**, 16302–16307.
23 S. Li, L. Fu, X. Xiao, H. Geng, Q. Liao, Y. Liao and H. Fu, *Angew. Chem., Int. Ed.*, 2021, **60**, 18059–18064.
24 Z. An, C. Zheng, Y. Tao, R. Chen, H. Shi, T. Chen, Z. Wang, H. Li, R. Deng, X. Liu and W. Huang, *Nat. Mater.*, 2015, **14**, 685–690.
25 H. Sun, Z. Xie, H. Wang, Y. Wu, B. Du, C. Guan and T. Yu, *J. Mater. Chem. C*, 2022, **10**, 8854–8859.
26 W. Dai, X. Niu, X. Wu, Y. Ren, Y. Zhang, G. Li, H. Su, Y. Lei, J. Xiao, J. Shi, B. Tong, Z. Cai and Y. Dong, *Angew. Chem., Int. Ed.*, 2022, **61**, e202200236.
27 X. Song, G. Lu, Y. Man, J. Zhang, S. Chen, C. Han and H. Xu, *Angew. Chem., Int. Ed.*, 2023, **62**, e202300980.
28 H. Ju, H. Zhang, L. X. Hou, M. Zuo, M. Du, F. Huang, Q. Zheng and Z. L. Wu, *J. Am. Chem. Soc.*, 2023, **145**, 3763–3773.
29 Y. Tao, R. Chen, H. Li, J. Yuan, Y. Wan, H. Jiang, C. Chen, Y. Si, C. Zheng, B. Yang, G. Xing and W. Huang, *Adv. Mater.*, 2018, **30**, 1803856.
30 J. Chen, X. Chen, L. Cao, H. Deng, Z. Chi and B. Liu, *Angew. Chem., Int. Ed.*, 2022, **61**, e202200343.
31 D. Li, F. Lu, J. Wang, W. Hu, X.-M. Cao, X. Ma and H. Tian, *J. Am. Chem. Soc.*, 2018, **140**, 1916–1923.
32 R. Kabe and C. Adachi, *Nature*, 2017, **550**, 384–387.
33 Z. Lin, R. Kabe, K. Wang and C. Adachi, *Nat. Commun.*, 2020, **11**, 191.
34 S. Xu, W. Wang, H. Li, J. Zhang, R. Chen, S. Wang, C. Zheng, G. Xing, C. Song and W. Huang, *Nat. Commun.*, 2020, **11**, 4802.
35 X. Zhang, L. Du, W. Zhao, Z. Zhao, Y. Xiong, X. He, P. F. Gao, P. Alam, C. Wang, Z. Li, J. Leng, J. Liu, C. Zhou, J. W. Y. Lam, D. L. Phillips, G. Zhang and B. Z. Tang, *Nat. Commun.*, 2019, **10**, 5161.
36 K. Jinnai, R. Kabe, Z. Lin and C. Adachi, *Nat. Mater.*, 2022, **21**, 338–344.
37 J. Li, X. Li, G. Wang, X. Wang, M. Wu, J. Liu and K. Zhang, *Nat. Commun.*, 2023, **14**, 1987.
38 H. A. Al-Attar and A. P. Monkman, *Adv. Funct. Mater.*, 2012, **22**, 3824–3832.
39 S. Hirata, K. Totani, J. Zhang, T. Yamashita, H. Kaji, S. R. Marder, T. Watanabe and C. Adachi, *Adv. Funct. Mater.*, 2013, **23**, 3386–3397.
40 D. Lee, O. Bolton, B. C. Kim, J. H. Youk, S. Takayama and J. Kim, *J. Am. Chem. Soc.*, 2013, **135**, 6325–6329.
41 S. Reineke, N. Seidler, S. R. Yost, F. Prins, W. A. Tisdale and M. A. Baldo, *Appl. Phys. Lett.*, 2013, **103**, 093302.
42 Z. Lin, R. Kabe, N. Nishimura, K. Jinnai and C. Adachi, *Adv. Mater.*, 2018, **30**, 1803713.
43 J. A. Li, L. Zhang, C. Wu, Z. Huang, S. Li, H. Zhang, Q. Yang, Z. Mao, S. Luo, C. Liu, G. Shi and B. Xu, *Angew. Chem., Int. Ed.*, 2023, **135**, e202217284.
44 Y. Li, L. Jiang, W. Liu, S. Xu, T. Y. Li, F. Fries, O. Zeika, Y. Zou, C. Ramanan, S. Lenk, R. Scholz, D. Andrienko, X. Feng, K. Leo and S. Reineke, *Adv. Mater.*, 2021, **33**, 2101844.
45 J. Guo, C. Yang and Y. Zhao, *Acc. Chem. Res.*, 2022, **55**, 1160–1170.
46 C. Qian, Z. Ma, X. Fu, X. Zhang, Z. Li, H. Jin, M. Chen, H. Jiang, X. Jia and Z. Ma, *Adv. Mater.*, 2022, **34**, 2200544.
47 Y. Li, G. Baryshnikov, F. Siddique, P. Wei, H. Wu and T. Yi, *Angew. Chem., Int. Ed.*, 2022, **61**, e202213051.
48 P. Han, G. Zhang, J. Wang, Y. Yao, Y. Qiu, H. Xu, A. Qin and B. Z. Tang, *CCS Chem.*, 2022, **5**, 1686–1696.
49 L. Ma, S. Sun, B. Ding, X. Ma and H. Tian, *Adv. Funct. Mater.*, 2021, **31**, 2010659.
50 C. Wang, Y. Zhang, Z. Wang, Y. Zheng, X. Zheng, L. Gao, Q. Zhou, J. Hao, B. Pi, Q. Li, C. Yang, Y. Li, K. Wang and Y. Zhao, *Adv. Funct. Mater.*, 2022, **32**, 2111941.
51 Y. Wang, J. Yang, M. Fang, Y. Gong, J. Ren, L. Tu, B. Z. Tang and Z. Li, *Adv. Funct. Mater.*, 2021, **31**, 2101719.
52 H. Thomas, D. L. Pastoetter, M. Gmelch, T. Achenbach, A. Schlögl, M. Louis, X. Feng and S. Reineke, *Adv. Mater.*, 2020, **32**, 2000880.
53 Y. Yang, J. Wang, D. Li, J. Yang, M. Fang and Z. Li, *Adv. Mater.*, 2021, **33**, 2104002.
54 M. Louis, H. Thomas, M. Gmelch, A. Haft, F. Fries and S. Reineke, *Adv. Mater.*, 2019, **31**, 1807887.
55 M. Louis, H. Thomas, M. Gmelch, F. Fries, A. Haft, J. Lindenthal and S. Reineke, *Adv. Opt. Mater.*, 2020, **8**, 2000427.
56 M. Gmelch, T. Achenbach, A. Tomkeviciene and S. Reineke, *Adv. Sci.*, 2021, **8**, 2102104.
57 R. Tian, S. M. Xu, Q. Xu and C. Lu, *Sci. Adv.*, 2020, **6**, eaaz6107.
58 Z. Huang, Z. He, B. Ding, H. Tian and X. Ma, *Nat. Commun.*, 2022, **13**, 7841.
59 Z. Wang, L. Gao, Y. Zheng, Y. Zhu, Y. Zhang, X. Zheng, C. Wang, Y. Li, Y. Zhao and C. Yang, *Angew. Chem., Int. Ed.*, 2022, **61**, e202203254.
60 B. Zhang, H. Li, J. Cheng, H. Ye, A. H. Sakhaei, C. Yuan, P. Rao, Y.-F. Zhang, Z. Chen, R. Wang, X. He, J. Liu, R. Xiao, S. Qu and Q. Ge, *Adv. Mater.*, 2021, **33**, 2101298.
61 C. Yang, M. Boorugu, A. Dopp, J. Ren, R. Martin, D. Han, W. Choi and H. Lee, *Mater. Horiz.*, 2019, **6**, 1244–1250.
62 Q. Hu, P. Zhang, Y. Zhang and J. Sun, *Molecules*, 2022, **27**, 8748.

63 Z. Xie, T. Yu, J. Chen, E. Ubba, L. Wang, Z. Mao, T. Su, Y. Zhang, M. P. Aldred and Z. Chi, *Chem. Sci.*, 2018, **9**, 5787–5794.
64 K. Xu, Y.-R. Jia, G.-L. Gao, H. jiang, X.-J. Liu and M. Xia, *Dyes Pigm.*, 2023, **211**, 111071.
65 W. W. H. Lee, Z. Zhao, Y. Cai, Z. Xu, Y. Yu, Y. Xiong, R. T. K. Kwok, Y. Chen, N. L. C. Leung, D. Ma, J. W. Y. Lam, A. Qin and B. Z. Tang, *Chem. Sci.*, 2018, **9**, 6118–6125.
66 A. Ajayaghosh, *Chem. Soc. Rev.*, 2003, **32**, 181–191.
67 J.-S. Ni, P. Zhang, T. Jiang, Y. Chen, H. Su, D. Wang, Z.-Q. Yu, R. T. K. Kwok, Z. Zhao, J. W. Y. Lam and B. Z. Tang, *Adv. Mater.*, 2018, **30**, 1805220.
68 S. Xu, Y. Duan and B. Liu, *Adv. Mater.*, 2020, **32**, 1903530.
69 N. J. Turro, V. Ramamurthy and J. C. Scaiano, *Principles of molecular photochemistry: An introduction*, University Science Books, Sausalito, Calif, USA, 2009.
70 C. Arivazhagan, A. Maity, K. Bakthavachalam, A. Jana, S. K. Panigrahi, E. Suresh, A. Das and S. Ghosh, *Chem.–Eur. J.*, 2017, **23**, 7046–7051.
71 J. Wang, Z. Chai, J. Wang, C. Wang, M. Han, Q. Liao, A. Huang, P. Lin, C. Li, Q. Li and Z. Li, *Angew. Chem., Int. Ed.*, 2019, **58**, 17297–17302.
72 J. Yuan, R. Chen, X. Tang, Y. Tao, S. Xu, L. Jin, C. Chen, X. Zhou, C. Zheng and W. Huang, *Chem. Sci.*, 2019, **10**, 5031–5038.
73 S. Song, X. Liu, E. Nikbin, J. Y. Howe, Q. Yu, I. Manners and M. A. Winnik, *J. Am. Chem. Soc.*, 2021, **143**, 6266–6280.
74 S. Yoshida and M. Trifkovic, *Macromolecules*, 2019, **52**, 7678–7687.
75 Z. Liu, T. Lu and Q. Chen, *Carbon*, 2020, **165**, 461–467.
76 T. Lu and F. Chen, *J. Comput. Chem.*, 2012, **33**, 580–592.
77 Y. Tao, C. Liu, Y. Xiang, Z. Wang, X. Xue, P. Li, H. Li, G. Xie, W. Huang and R. Chen, *J. Am. Chem. Soc.*, 2022, **144**, 6946–6953.
78 X. Yan, H. Peng, Y. Xiang, J. Wang, L. Yu, Y. Tao, H. Li, W. Huang and R. Chen, *Small*, 2021, **18**, 2104073.
79 B. Zhang, H. Li, J. Cheng, H. Ye, A. H. Sakhaei, C. Yuan, P. Rao, Y.-F. Zhang, Z. Chen, R. Wang, X. He, J. Liu, R. Xiao, S. Qu and Q. Ge, *Adv. Mater.*, 2021, **33**, 2101298.
80 S. Deng, J. Wu, M. D. Dickey, Q. Zhao and T. Xie, *Adv. Mater.*, 2019, **31**, 1903970.
81 G. D. Zhu, Y. Hou, J. Xu and N. Zhao, *Adv. Funct. Mater.*, 2021, **31**, 2007173.
82 F. Gholami, L. Yue, M. Li, A. Jain, A. Mahmood, M. Fratarcangeli and R. Ramprasad, *Adv. Mater.*, 2024, **36**, 2408774.